Amino Acids (2010) 39:399–408
DOI 10.1007/s00726-009-0453-2

ORIGINAL ARTICLE

Efficient expression of human soluble guanylate cyclase in *Escherichia coli* and its signaling-related interaction with nitric oxide

Fangfang Zhong · Hongyan Wang · Tianlei Ying · Zhong-Xian Huang · Xiangshi Tan

Received: 22 November 2009 / Accepted: 17 December 2009 / Published online: 9 January 2010

Abstract Soluble guanylate cyclase (sGC), as a nitric oxide (NO) sensor, is a critical heme-containing enzyme in NO-signaling pathway of eukaryotes. Human sGC is a heterodimeric hemoprotein, composed of a α-subunit (690 AA) and a heme-binding β-subunit (619 AA). Upon NO binding, sGC catalyzes the conversion of guanosine 5′-triphosphate (GTP) to 3′,5′-cyclic guanosine monophosphate (cGMP). cGMP is a second messenger and initiates the nitric oxide signaling, triggering vasodilatation, smooth muscle relaxation, platelet aggregation, and neuronal transmission etc. The breakthrough of the bottle neck problem for sGC-mediated NO singling was made in this study. The recombinant human sGC β1 subunit (HsGCβ619) and its truncated N-terminal fragments (HsGCβ195 and HsGCβ384) were efficiently expressed in *Escherichia coli* and purified successfully in quantities. The three proteins in different forms (ferric, ferrous, NO-bound, CO-bound) were characterized by UV–vis and EPR spectroscopy. The homology structure model of the human sGC heme domain was constructed, and the mechanism for NO binding to sGC was proposed. The EPR spectra showed a characteristic of five-coordinated heme-nitrosyl species with triplet hyperfine splitting of NO. The interaction between NO and sGC was investigated and the schematic mechanism was proposed. This study provides new insights into the structure and NO-binding of human sGC. Furthermore, the efficient expression system of *E. coli* will be beneficial to the further studies on structure and activation mechanism of human sGC.

Keywords Human soluble guanylate cyclase · NO sensor · NO signal transduction · *E. coli* expression system

Electronic supplementary material The online version of this article (doi:10.1007/s00726-009-0453-2) contains supplementary material, which is available to authorized users.

F. Zhong · T. Ying · Z.-X. Huang
Department of Chemistry, Fudan University, 200433 Shanghai, China

H. Wang
Institutes of Biomedical Sciences, Fudan University, 200433 Shanghai, China

X. Tan (✉)
Department of Chemistry and Institutes of Biomedical Sciences, Fudan University, 200433 Shanghai, China
e-mail: xstan@fudan.edu.cn

Introduction

The Nobel Prize in physiology and medicine in 1998 was awarded to R. F. Furchgott, L. J. Ignarro, and F. Murad for their discovery of "the nitric oxide (NO) as a signaling molecule in the cardiovascular system". This stimulated intense interests of scientists in the study on soluble guanylate cyclase (sGC) mediated NO-signaling system. In the past decade, there were more than 3,000 papers published in this area. sGC, as a nitric oxide sensor, is a critical heme-containing enzyme in NO-signaling pathway of eukaryotes. Upon NO binding, sGC catalyzes the conversion of guanosine 5′-triphosphate (GTP) to 3′,5′-cyclic guanosine monophosphate (cGMP). cGMP, as an important second messenger, regulates several effector proteins and plays an important role in many physiological processes, for example, vasodilatation, smooth muscle relaxation, platelet aggregation, and neuronal transmission (Chen et al. 2008; Denninger and Marletta 1999; Evgenov et al. 2006; Sarkar et al. 2008; Wang-Rosenke et al. 2008). Dysfunction of NO

signaling results in many pathological disorders, ranging from several cardiovascular diseases, such as arterial hypertension, pulmonary hypertension, heart failure, atherosclerosis and restenosis, to neurodegenerative diseases (Evgenov et al. 2006). sGC in eukaryote is a heterodimeric hemoprotein, composed of a α-subunit and a heme-binding β-subunit. For human sGC, there are two isoforms in vivo (Kosarikov et al. 2001a, b): α1β1 and α2β2, while the α1β1 heterodimer is the more abundant. The prosthetic heme moiety, crucial for NO sensing, is located in the heme-binding domain of the β subunit (Evgenov et al. 2006; Pellicena et al. 2004; Schmidt et al. 2004). Up to now there is no crystal structure of sGC in eukaryotes, even through the crystal structures of H-NOX (Heme Nitric oxide/OXygen) domain from bacteria, *Nostoc* sp and *Thermoanaerobacter Tengcongensis* (Ma et al. 2007; Nioche et al. 2004; Pellicena et al. 2004; Winger et al. 2008) and the catalytic domain of sGC from the green algae *Chlamydomonas reinhardtii* (Winger et al. 2008), were reported in recent years. Furthermore, the structure and property of H-NOX domain are different from those of human sGC and the H-NOX domain cannot be used as the model of NO-bound heme domain of human sGC. The structure and mechanism of activation and/or stimulation of sGC upon the NO binding is still poorly understood in spite of several models have been proposed (Ballou et al. 2002; Bellamy et al. 2002; Stone and Marletta 1996; Zhao et al. 1999). The detailed information of the structure and mechanism on sGC-mediated NO-signaling was limited for lacking of purified sGC in quantities, which do indeed impede further investigation into the structure–function relationship, and consequently, the development of sGC-specific drugs of cardiovascular disease. This has been extremely challenging in the history of sGC research. How to obtain pure human sGC protein in quantities is the bottle neck for the study on sGC-mediated NO signaling.

Originally, sGC was isolated from a number of mammalian tissues, mainly bovine and rat lungs (Ignarro et al. 1982; Makino et al. 2003; Mathis et al. 2008; Ohlstein et al. 1982; Stone and Marletta 1996; Stone et al. 1995; Wolin et al. 1982). In the case of human isoforms, direct isolation from native sources becomes virtually impossible. To this end, the *Escherichia coli* expression system is the most desired to overexpress sGC. As for eukaryotic sGC, the expression of truncated rat lung heme-binding domain and catalytic domain in *E. coli* was achieved with limited yield by Marletta et al., but the full-length β1 (619 residues) subunit failed (Karow et al. 2005; Winger and Marletta 2005; Zhao and Marletta 1997). Recently, Hu et al. expressed and characterized an insect sGC from *Manduca sexta* (Hu et al. 2008). However, as far as human isoforms of sGC are concerned, attempts to overexpress the functional enzyme in *E. coli*, even any truncated domain, have not been successful so far. Although the functional expression of recombinant human sGC was achieved in the baculovirus/Sf9 cells (Kosarikov et al. 2001a, b; Lee et al. 2000; Zabel et al. 1998), the yield of human sGC was relatively limited.

Herein, we report, for the first time, the recombinant human sGC β1 subunit in full-length (HsGCβ619) and its truncated N-terminal fragments with 195 and 384 residues (HsGCβ195 and HsGCβ384), which were overexpressed in *E. coli* and purified successfully with a yield of 20 mg/L of cell culture. The three proteins in different states (ferric, ferrous, NO-bound, CO-bound) were fully characterized by UV–vis and EPR spectroscopy. The homology model of human sGC heme domain was constructed, and a scheme for NO binding to sGC based on the experimental results was proposed.

Materials and methods

Materials

Plasmid FL14116 containing the entire human sGC β1 cDNA was purchased from Fulengen Company, China. The MBPHT-mCherry2 vector was a kind gift from Dr. Yu Ding (School of Life Sciences, Fudan University). The TEV protease expression vector pRK1043 and the *E. coli* strain XL10-Gold and Rosetta (DE3) pLysS were obtained from Novagen. *Pfu* DNA polymerase, T4 DNA ligase, dNTP and restriction enzymes (*Bam*HI, *Hin*dIII, *Eco*RI, *Xho*I) were purchased from New England Biolabs. Oligonucleotide PCR primer pairs, labeled as P1, P2, and P3, were synthesized and DNA sequencing reactions were performed by Shanghai Invitrogen Biotech Co. Ltd. The plasmid purification kits, gel extraction kits, Nickel–nitrilotriacetic acid (Ni–NTA) resin and Sephadex G-25 resin were purchased from Qiagen (Chatsworth, CA). Superdex^{TM} 200 HiLoad^{TM} 16/60 gel filtration column was from Pharmacia. Carbon monoxide was from Matheson. diethylammonium (Z)-1-(*N*,*N*-diethylamino) diazen-1-ium-1,2-diolate (DEA/NO) was purchased from J&K Chemical Ltd. All other reagents were of analytic grade.

P1 [5′-ATGGATCCGGCGGCGGCAGCGGTATGTACGGATTTGTGAATC-3′(F); 5′-CCCAAGCTTTCAAAGATCTTCATAAAAATCC-3′(R)]

P2 [5′-CGAATTCGAAAACCTGTATTTTCAGGGCGGCGGCAGCGGTATGTACGGATTTG-3′(F); 5′-CCTCTCGAGTCAGTGATGGTGATGGTGATGTTCCAGGGCTCTTAAC-3′(R)]

P3 [5′-CGAATTCGAAAACCTGTATTTTCAGGGCGGCGGCAGCGGTATGTACGGATTTG-3′(F); 5′-CCTCTCGAGTCAGTGATGGTGATGGTGATGGTCATCATCCTGC-3′(R)]

Subcloning of *HsGCβ195, HsGCβ384* and *HsGCβ619*

Standard molecular cloning techniques were employed throughout. *HsGCβ195*, *HsGCβ384* and *HsGCβ619* (encoding human sGC β1 N-terminal fragment cDNA residues 1–195, 1–384, and 1–619, respectively) were amplified using plasmid FL14116 containing the entire human sGC β1 cDNA as template. PCR products were obtained using the primer pair P1 for *HsGCβ195*, P2 for *HsGCβ384*, and P3 for *HsGCβ619*, respectively. The forward and reverse primers were designed to introduce *Bam*HI and *Hin*dIII restriction sites for *HsGCβ195*, *Eco*RI and *Xho*I restriction sites for *HsGCβ385* (or *HsGCβ619*), a TEV protease recognition site and hexa-His peptide sequence for *HsGCβ385* (or *HsGCβ619*), respectively. The resulting PCR products were purified and subsequently digested, respectively. The digested PCR products were ligated with T4 DNA ligase to linearized MBPHT-mCherry2 vector that had been digested with *Bam*HI/*Hin*dIII for *HsGCβ195*, and *Eco*RI/*Xho*I for *HsGCβ384* and *HsGCβ619*, respectively. The resulting ligation mixture was transformed into XL10-Gold competent cells by heat shock. The constructed plasmids of *HsGCβ195, HsGCβ384* and *HsGCβ619* were verified by DNA sequencing.

Expression of *HsGCβ195, HsGCβ384* and *HsGCβ619* in *E. coli*

The three proteins HsGCβ195, HsGCβ384 and HsGCβ619 were expressed, respectively with the following procedure. Plasmids were transformed into *E. coli* Rosetta (DE3) pLysS competent cells by heat shock. A single colony from Luria–Bertani (LB)-agar plate containing 50 μg/ml ampicillin and 34 μg/ml chloramphenicol was selected and then applied to inoculate 3 ml of LB media containing 50 μg/ml ampicillin and 34 μg/ml chloramphenicol. The start culture, which was incubated at 37°C for 8 h, was transferred to 250 ml of modified Terrific Broth (M-TB, added with 20 mM Glucose, 2 g/L $NaNO_3$) containing 50 μg/ml ampicillin and 34 μg/ml chloramphenicol. Cultures were incubated at 37°C until its OD_{600} reached 0.8, then the incubation temperature was lowered to 20°C and the protein overexpression was induced with 0.1 mM IPTG. The cells were allowed to grow overnight at 20°C and harvested by centrifugation. The cell pellets were frozen and stored at −80°C.

Protein purification and heme reconstitution

HsGCβ195 was purified as follows: the frozen cell pellets were thawed on ice, resuspended in 5 ml/g buffer A (50 mM Na–Pi, 500 mM NaCl, 5 mM β-mecaptoethanol (β-Me), 20% glycerol, pH 8.0) with 2 mg/ml lysozyme and 1 mM phenyl methyl sulfonyl fluoride (PMSF), and lysed by sonication for 5 min on ice. The resulting cell homogenate was centrifuged. The supernatant from this centrifugation was applied to Ni–NTA column that had been equilibrated with buffer A. The Ni–NTA column was washed with 10 column volume of buffer A containing 5 mM imidazole and then the protein was eluted with two column volume of buffer A containing 150 mM imidazole. The imidazole in the elute was removed by dialyzing with a large amount of buffer A overnight at 4°C. After cleavage of the N-terminal maltose binding protein (MBP) tag by TEV protease, the protein solution was subjected to Ni–NTA column again to remove the MBP tag by bonding to the Ni–NTA column. The apo-HsGCβ195 in buffer A containing 5 mM DTT was used to reconstitute with heme by adding five equivalents of hemin stock at 4°C overnight. The HsGCβ195–Hemin mixture was concentrated and then applied to the column (1 × 20 cm) of Sephadex G-25 equilibrated with buffer B (50 mM Tris–HCl, pH 8.0) to remove the unbound heme. The elution fractions from the Sephadex G-25, identified by a characteristic of deep red-brown color and UV–vis spectrum, were pooled and concentrated, and then subjected to the Superdex^{TM} 200 HiLoad^{TM} 16/60 gel filtration column equilibrated with buffer C (50 mM Tris–HCl, 100 mM NaCl, pH 8.0). Fractions containing HsGCβ195 were collected, frozen in liquid nitrogen and stored at −80°C.

HsGCβ384 and HsGCβ619 were purified as described for HsGCβ195 with the following modifications. The Ni–NTA column containing HsGCβ384 or HsGCβ619 was washed with 10 column volume of buffer A containing 20 mM imidazole and then eluted with two column volume of buffer A containing 250 mM imidazole. All proteins obtained were over 95% pure, based on imaging Coomassie-Blue stained 15% SDS–PAGE gels (Fig. 1). The protein concentration was determined by the Bradford method using BSA as the standard, and the heme concentration in the protein samples was measured by the pyridine-hemochromagen assay with an extinction coefficient of $\varepsilon_{R-O,\ 557-540} = 22.1\ mM^{-1}cm^{-1}$ (Berry and Trumpower 1987).

Simulation of molecular structure of HsGCβ195

The initial coordinates for HsGCβ195 were constructed based on the crystal structure of the H-NOX domain of *Nostoc* sp (*Ns* HNOX) (pdb entry: 2O09) (Ma et al. 2007) via homology-modeling (http://swissmodel.expasy.org/SWISS-MODEL.html). Water molecules in the crystal structure were retained in the simulation. Force field parameters for heme were adopted, which were published before (Autenrieth et al. 2004; Laidig and Daggett 1996) and the peptide was simulated with CHARMM force field (Mackerell et al. 2004, 1998). The structure was first

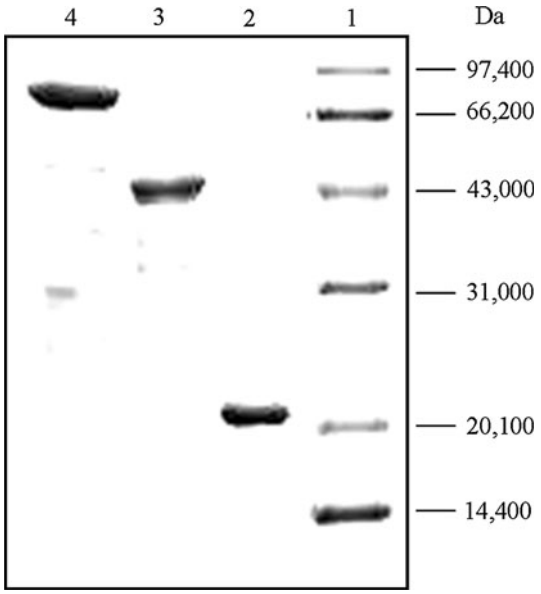

Fig. 1 SDS–PAGE of purified human sGC constructs. *Lane 1* Marker, *Lane 2* HsGCβ195, *Lane 3* HsGCβ384, *Lane 4* HsGCβ619

minimized for 1,000 steps with conjugate gradient method, and equilibrated for 10 ps with the time step of 1 fs, then was further minimized for 180,000 steps. NAMD (not just a molecular dynamics) program was used for simulations, and VMD (visual molecular dynamics) program was employed for structural analysis.

UV–vis and EPR spectroscopy

Electronic absorption spectra of these three proteins in buffer D (50 mM Hepes at pH 7.4, 50 mM NaCl), were recorded in an anaerobic cuvette on a HP8453 UV–visible spectrophotometer. The protein concentration was 3 μM. Protein samples were prepared in a highly pure N_2-atmosphere glove box (MBraun). The ferrous proteins were obtained by adding 1 mM Ti^{3+}-citrate or 10 mM dithionite. The NO–bound protein complexes were produced by bubbling excess NO into the protein solution for 5 min, which was generated by the reaction of $NaNO_2$ and HCl, and passed through an aqueous solution of sodium hydroxide (NaOH) to eliminate possible contamination of acid and higher oxides of nitrogen. The CO-bound complexes were generated by bubbling CO (carbon monoxide) through the protein samples for 5 min.

X-band EPR spectra were recorded at 100 K on a Bruker BioSpin GmbH spectrometer. The spectra were recorded under the following conditions: microwave frequency, 9.44 GHz; microwave power, 2.0 mW; modulation frequency, 100 kHz; modulation amplitude, 4.00 G; and time constant, 163.84 ms. The concentrations of the samples were 120, 60 and 100 μM for HsGCβ195, HsGCβ384 and HsGCβ619, respectively, in buffer D. NO–bound protein complexes of HsGCβ195, HsGCβ384 and HsGCβ619 were prepared anaerobically in the glove box under highly pure N_2 atmosphere. The protein was reduced with excess sodium dithionite, bubbled with NO in a sealed cuvette with a rubber septum for 5 min, and then transferred with a steel needle into an EPR tube. The samples in the EPR tubes were quickly frozen in liquid nitrogen for EPR measurements.

DEA/NO binding experiments

The HsGCβ proteins in buffer D and DEA/NO stock in 10 mM NaOH were prepared in a high purity N_2-atmosphere glove box. The ferrous HsGCβ protein, which was reduced with 1 mM Ti^{3+}-citrate, was transferred into an anaerobic cuvette with a rubber septum. The desired concentration of DEA/NO solution was prepared by diluting the DEA/NO stock solution with buffer D and incubated for at least 30 min. The reaction was initiated by adding the DEA/NO solution to the protein with a syringe, and monitored by electronic absorption spectroscopy on a HP8453 UV–visible spectrophotometer with kinetic mode at 14°C. The final concentrations were 1.5 and 7.5 μM for the HsGCβ protein and DEA/NO, respectively. Data collection was started from the addition of DEA/NO solution. Spectra were recorded every 2 s for the first 2 min, every 1 min for the later 20 min and every 5 min thereafter for a total of 3 h, or until the reaction reached the equilibrium.

Results and discussion

Cloning, expression and purification

The genes encoding human sGC β1 subunit HsGCβ619 or its truncated fragments HsGCβ195 and HsGCβ384 were subcloned successfully into the MBPHT-mCherry2 vector, respectively. This is the first report that the human sGC β1 and its fragments were expressed in *E. coli*. After the MBP tag was removed by TEV protease, all three proteins remained soluble. The final yield of each protein was at least 20 mg/L of cell culture. The three proteins displayed an A_{soret}/A_{280} ratio of about 1.7. The highly efficient *E. coli* expression system of HsGCβ is critical to the study of the structure, function and catalytic mechanism of human sGC.

The results showed that the MBP tag indeed makes great contribution to the satisfactory expression of soluble fusion proteins. Besides, the host strain (Rosetta (DE3) pLysS), extremely rich media (mainly the 20 mM Glucose added in the TB media) and lower incubation temperature (20°C) did play crucial roles in the overexpression of soluble fusion proteins.

Marletta et al. (Karow et al. 2005; Zhao and Marletta 1997) reported that the truncated rat β1–385 (residues 1–385), when isolated, was a homodimer due to the short stretch of amino acid residues (residues 340–385), and the truncated rat β1–194 (residues 1–194) was found to be readily oxidized and aggregated. In this study, for human sGC, we found that HsGCβ195 mainly existed in dimer, while for HsGCβ384 or HsGCβ619, the major form appeared to be oligomer, indicated by the results of Superdex^{TM} 200 HiLoad^{TM} 16/60 gel filtration column.

Homology model of human HsGCβ195

No crystal structure of sGC of higher eukaryotes has so far been reported, while two heme domain orthologs of sGC from prokaryotes (*Tt* H-NOX domain (Nioche et al. 2004; Pellicena et al. 2004) and *Ns* H-NOX domain (Ma et al. 2007)) have been published. The H-NOX domains from *Tt* and *Ns* have sequence identity of 18 and 33% with that of HsGCβ195. The *Ns* H-NOX domain was demonstrated to share similar ligand binding properties with eukaryote sGC and likewise postulated to be evolutionarily homologous to eukaryote sGC, suggesting that the crystal structure of the *Ns* H-NOX domain should be a better template for homology modeling of the sGC heme domain than *Tt* H-NOX domain. Here, based on the recently published crystal structure of *Ns* H-NOX domain (pdb entry: 2O09) (Ma et al. 2007), the homology model of HsGCβ195 was constructed, shown in Fig. 2.

The conformational transformation of L2 (Loop2, residues 124–130) is identified as the primary response to the cleavage of the Fe-His bond of the H-NOX domain, perhaps from which the activation information is propagated from the H-NOX domain to the cyclase domain (Capece et al. 2008). As shown in Fig. 2, the HsGCβ195 and *Ns* H-NOX domain possess the similar fold features, but there is an obvious difference in the L2. The L2 in HsGCβ195 becomes more flexible than that in *Ns* H-NOX domain, possibly favorable for the transition from the heme pocket conformational change to the catalytic activity in the evolutionary perspective.

UV–visible spectra

The electronic absorption spectra of HsGCβ195, HsGCβ384, and HsGCβ619 in different forms are presented in Fig. 3. The absorption peaks and extinction coefficients are summarized in Table 1.

The resting and activated states of other sGCs were investigated spectroscopically with resonance Raman (RR) (Deinum et al. 1996; Fan et al. 1998; Li et al. 2005; Tomita et al. 1997; Vogel et al. 1999; Yu et al. 1994) and electronic absorption spectroscopy (Burstyn et al. 1995; Karow et al. 2005; Lee et al. 2000; Stone and Marletta 1994; Vogel et al. 1999; Zhao and Marletta 1997). Two kinds of sGCs, named as sGC1 (heme-reconstituted) and sGC2 (as-isolated) were reported by Vogel et al. (1999). The ferrous heme in sGC2 was demonstrated to be absolutely in five-coordinated high-spin state, while that in sGC1 presented a mixture of five-coordinated high-spin and six-coordinated low-spin state.

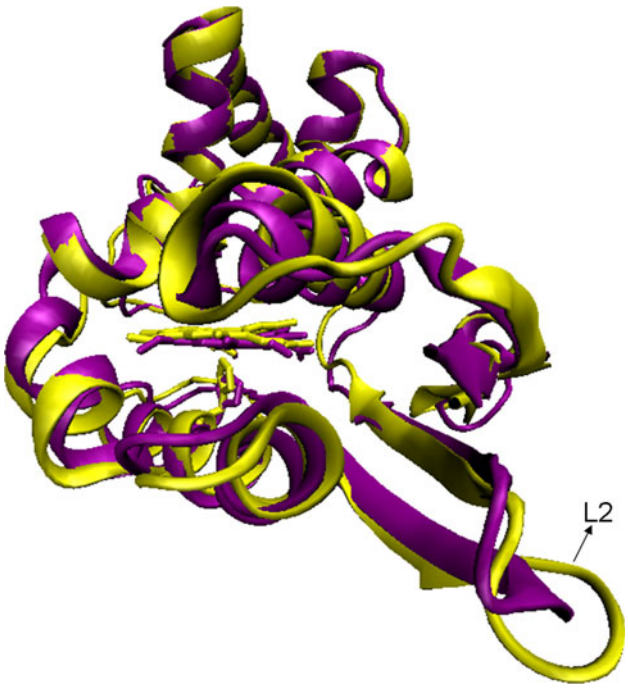

Fig. 2 Homology model of the heme-binding domain of the human sGC β1 subunit (HsGCβ195), revealing the changes of L2 (Loop2, residues 124–130) between the structure of *Ns* H-NOX domain (the H-NOX domain of *Nostoc* sp) and HsGCβ195. *Yellow* HsGCβ195; *purple Ns* H-NOX domain (pdb entry: 2O09)

The ferric forms

The ferric HsGCβ195 and HsGCβ384 have the similar spectra features with a Soret peak at 409 nm, while the ferric HsGCβ619 contains a Soret peak centered at 397 nm. The previous studies on hemoproteins suggested that the Soret peaks of ferric heme at 390–400, 405–410 and 410–425 nm correspond to the five-coordinated high-spin, six-coordinated high-spin and six-coordinated low-spin state, respectively (Antonini and Brunori 1971; Stone and Marletta 1994; Yamanaka 1992). On the basis of the UV–vis spectra, it is inferred that both the HsGCβ195 and HsGCβ384 may contain a six-coordinated high-spin ferric heme center, and HsGCβ619 contains a five-coordinated high-spin ferric heme.

The spectrum of HsGCβ619 is similar to those previously reported, in which the Soret peak was at 393 nm for the as-isolated bovine sGC and rat β1(1-385) by Marletta

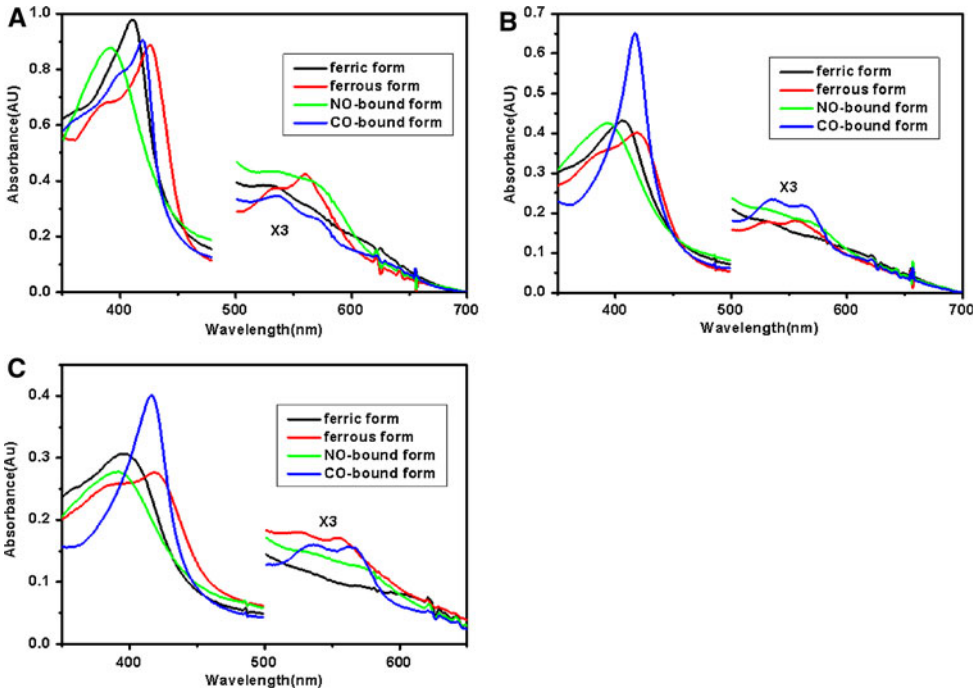

Fig. 3 Electronic absorption spectra of (**a**) HsGCβ195, (**b**) HsGCβ384, (**c**) HsGCβ619, showing the Soret peak and α/β region. The heme concentration was 3 μM in 50 mM Hepes at pH 7.4, 50 mM NaCl

Table 1 UV–vis spectra data for HsGCβ195, HsGCβ384 and HsGCβ619

Protein	Soret (ε)	β (ε)	α (ε)
Ferric form			
HsGCβ195	409 (209)		
HsGCβ384	409 (194)		
HsGCβ619	397 (156)		
Ferrous form			
HsGCβ195	425 (189)	533 (27)	560 (30)
HsGCβ384	418 (181)	530 (27)	555 (27)
HsGCβ619	418 (145)	525 (28)	554 (27)
NO-bound form[a]			
HsGCβ195	393 (187)		
HsGCβ384	392 (191)		
HsGCβ619	392 (141)		
CO-bound form			
HsGCβ195	420 (193)	535 (25)	569 (19)
HsGCβ384	417 (293)	534 (35)	560 (33)
HsGCβ619	416 (204)	536 (27)	561 (26)

All peak positions are in nm. All molecular extinction coefficients are in $mM^{-1}cm^{-1}$. *HsGCβ195* truncated human sGC β1 subunit with 1–195 residues, *HsGCβ384* truncated human sGC β1 subunit with 1–384 residues, *HsGCβ619* full-length human sGC β1 subunit with 1–619 residues

[a] The values for NO-bound form in the table are measured in the case of sodium dithionite as reductant, when the NO-bound sGC constructs are reduced with Ti^{3+}-citrate, the Soret peak for the three proteins is at 398 nm

et al. (Stone and Marletta 1994; Zhao and Marletta 1997). But Burstyn et al. (1995) showed that the Soret peak was at 420 nm for the as-isolated and heme-reconstituted bovine sGC. As noted above, the spectral characteristics of ferric HsGCβ195 and HsGCβ384 differ significantly from those of HsGCβ619. The difference possibly resulted from the different distal heme environment for the N-terminal fragments and the full-length β1 construct. Furthermore we proposed that the C-terminal fragment of sGC located around the distal pocket and therefore sterically hindered the sixth coordination position. But, up to date, it is not clear what is the exact sixth ligand of HsGCβ195 and HsGCβ384, perhaps histidine (Burstyn et al. 1995), or some other endogenous or exogenous ligands.

The ferrous forms

Upon the reduction with excessive sodium dithionite or with Ti^{3+}-citrate, the Soret band shifted to 425 nm and the broad α/β band was replaced by observable α/β bands at 560 and 533 nm for HsGCβ195, which is identical to that of sGC1 studied previously (Burstyn et al. 1995; Vogel et al. 1999). The HsGCβ384 and HsGCβ619 exhibited the similar spectra, showing the Soret peak shift to 418 nm and the appearance of split α/β bands at 555 and 530 nm. The ferrous human sGC species indicated a mixture of six-coordinated low-spin and five-coordinated high-spin heme iron, which is similar to that previously observed (Burstyn

et al. 1995; Gerzer et al. 1981; Vogel et al. 1999). The variations in the Soret position of the three proteins were due to the difference of distal heme pocket environment. Along with the reduction of the protein, some changes occurred in conformation and the spin state of the central heme iron.

The NO-bound forms

The three proteins showed the similar spectra features when they were reduced with sodium dithionite and saturated with NO, exhibiting broadened Soret peak at 393 nm, and weak α/β bands at 530 and 565 nm. However, when the samples were anaerobically reduced with Ti^{3+}-citrate, and then saturated with NO, the Soret peak shifted to 398 nm, which is identical to what previously reported (Burstyn et al. 1995; Gerzer et al. 1981; Ignarro et al. 1986; Vogel et al. 1999), suggesting that the NO–protein complexes were in a five-coordinated high-spin state. The results implied that Ti^{3+}-citrate may be the better reductant for obtaining the NO-bound ferrous sGC forms. It is possible that the heme pocket slightly changed due to the reaction between NO and sodium dithionite in the presence of sodium dithionite (Cary et al. 2005; Kharitonov et al. 1997; Winger et al. 2007).

The CO-bound forms

The addition of CO to the anaerobically reduced HsGCβ195 resulted in the Soret band shifting to 420 nm, with a slightly decrease of intensity, and observable α/β bands at 535 and 569 nm. HsGCβ384 and HsGCβ619 shared the similarity in the spectra of CO-protein complexes. The CO complexes exhibited a sharp Soret band at 417 nm, with an extremely concomitant increase in the extinction coefficient, and split α/β bands at 535 and 560 nm. These data suggested that the CO complexes are in six-coordinated low-spin state (Burstyn et al. 1995; Gerzer et al. 1981; Stone and Marletta 1994; Vogel et al. 1999).

From all the above observations, HsGCβ195, HsGCβ384 and HsGCβ619 in the resting states (ferric and ferrous unbound species) possess slightly different spectral features with one another and with those in previous reports (Burstyn et al. 1995; Karow et al. 2005; Lee et al. 2000; Stone and Marletta 1994; Vogel et al. 1999; Zhao and Marletta 1997), suggesting different ligation states and distal heme pockets. But we cannot hereby come to the conclusion that the proteins here are misfolded and not in their functional states. The first of all, the spectral differences in the resting state between sGC1 (heme-reconstituted) and sGC2 (as-isolated) indeed exist as reported by Burstyn et al. It is possible that the heme of sGC1 was not properly refolded by heme reconstitution, but on the other hand, maybe the heme pocket is partially disrupted by the loss of the sixth ligand in the isolation of sGC2. The second, as we know, the conformational change is critical for the sGC activation. From the above spectral results, in the activated states (NO-bound and CO-bound species), the three HsGCβ proteins show similar spectra features, indicating that they respond similarly to the presence of NO and CO. That is to say, not only can NO and CO bind to the HsGCβ proteins, but also trigger the following conformational change successfully. Therefore, we conclude that the differences in the resting states do not affect the activation properties, which was suggested in previous studies (Vogel et al. 1999), and the proteins we obtained are functional. Furthermore, the experimental results in this work provides some new insights into the structure and NO-binding of sGC.

EPR experiment

The EPR spectra of the freeze-trapped samples are shown in Fig. 4, suggesting that the NO-complexes of three proteins share similar properties. The NO complexes exhibited g values of $g_x = 2.009$, $g_z = 2.068$ with triplet hyperfine splitting of NO, characteristic of five-coordinated heme-nitrosyl species (Makino et al. 1999, 2003; Nioche et al. 2004; Stone et al. 1995; Yazawa et al. 2006). These data showed that the heme in the N-terminal fragment (195, or 384) had the similar features of NO binding to that of the

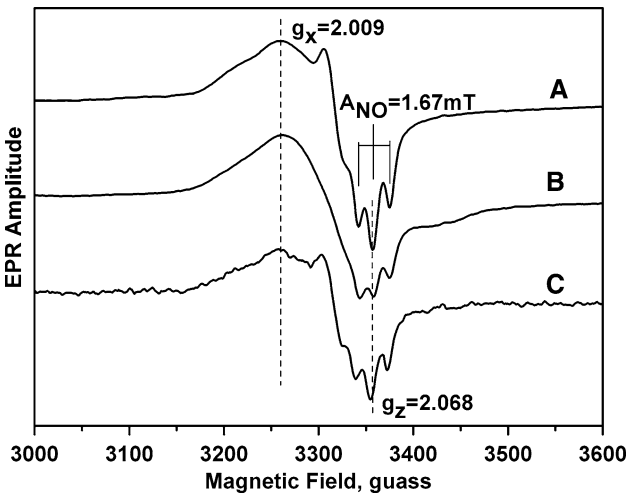

Fig. 4 EPR spectra of the NO bound sGC of (**a**), HsGCβ195; (**b**), HsGCβ619; (**c**), HsGCβ384. The concentrations of the samples were 120, 100 and 60 μM for HsGCβ195, HsGCβ619 and HsGCβ384, respectively, in 50 mM Hepes at pH 7.4, 50 mM NaCl. The EPR conditions were as follows: temperature, 100 K; microwave frequency, 9.44 GHz; microwave power, 2.00 mW; modulation frequency, 100 kHz; modulation amplitude, 4.00 G; and time constant, 163.840 ms

full-length β1 and the as-isolated heterodimer sGC. Therefore, the heme-binding domain of human sGC HsGCβ195 or HsGCβ384, as an excellent tool, can be used to further characterize the sGC heme pocket and study the NO activation/deactivation mechanism.

DEA/NO binding process

The changes of UV/Vis spectra when DEA/NO binding to HsGCβ195 or HsGCβ619 were shown in Fig. 5. For HsGCβ195, within 2 s, the Soret peak shifted to 406 nm from 425 nm. In the next 1 min the Soret peak gradually shifted to 420 from 400 nm through one set of isosbestic points at 412 nm, following the absorbance at 400 nm decreased, which indicated the formation of a six-coordinated state. After that, the absorbance at 420 nm gradually decreased with an accompanying increase at 398 nm, showing that the six-coordinated NO complex was converted to one five-coordinated form. About 20 min later, the absorbance at 398 nm decreased with an accompanying increase at 425 nm, which may result from the slow dissociation of the NO complex. The spectral changes indicated that HsGCβ619 possessed the similar characteristics to HsGCβ195 in the DEA/NO binding process, but the conversion of six-coordinated NO complex to the five-coordinated form and the following dissociation of NO complex were much slower than HsGCβ195 (Fig. 5).

Based on these observations, the possible mechanism for the transition between different HsGCβ forms, shown in Fig. 6, was proposed for the DEA/NO binding process. The state A with a Soret peak at 425 nm represents the unbound ferrous sGC, six-coordinated low-spin state. The distal ligand could be a histidine (Burstyn et al. 1995), as shown in Fig. 6. Several seconds after the mixing with DEA/NO, both the axial ligands were removed in the presence of NO, and NO binds to the distal site of the heme, resulting in the Soret peak shift to about ~400 nm and the conformational change in the heme pocket. Then, the second NO bound to the proximal site of the heme, leading to the formation of dinitrosyl-heme (state C) (Lorkovic and Ford 2000; Russwurm and Koesling 2004). From the unstable dinitrosyl-heme, one NO was released, resulting in five-coordinated NO complexes (state D). But whether the NO bound was in the proximal site or the distal site was not identified (Ballou et al. 2002; Russwurm and Koesling 2004). Several hours later, the NO gradually dissociated from the NO–protein complex and returned back to the original state A. As depicted in the scheme, the state B and state D possess the similar five-coordinated NO-bound heme with the slight difference in the Soret band position, due to the slight perturbation of the heme pocket.

According to the time courses of absorbance changes at 398, 420 and 425 nm (as shown in Fig. S1), rate constants of the A → B, B → C, C → D, D → A steps were

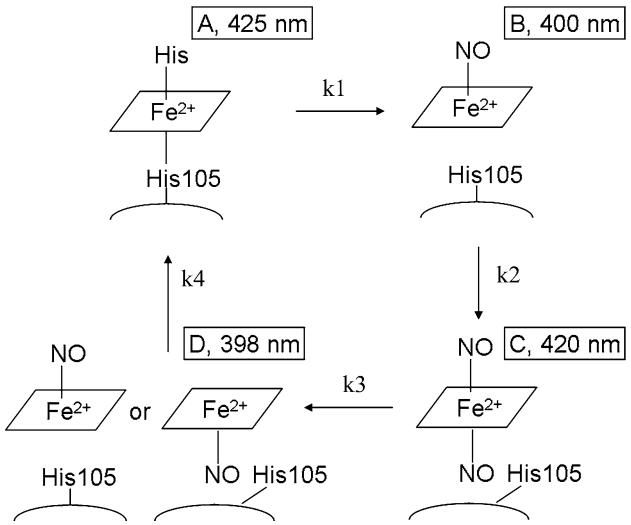

Fig. 6 A scheme for NO binding to sGC. Further explanation of the scheme is given in "Results and discussion"

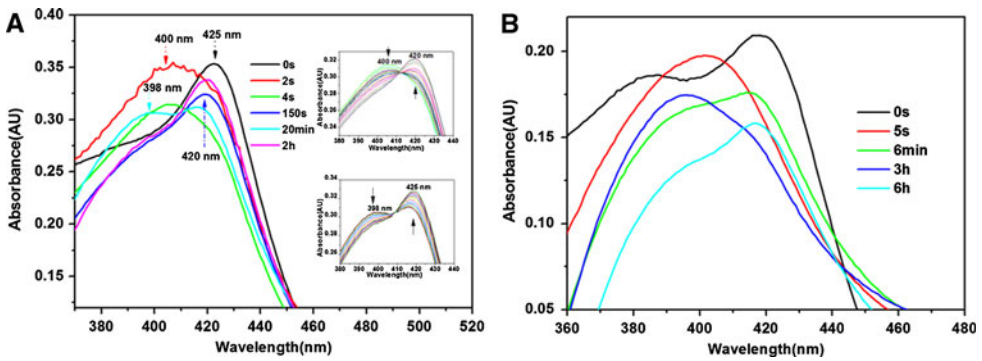

Fig. 5 Spectral changes in the ferrous sGC, reduced with 1 mM Ti^{3+}-citrate, followed by rapid mixing with NO recorded on UV–visible spectrophotometer. The final concentrations of sGC and DEA/NO (diethylammonium (Z)-1-(*N*,*N*-diethylamino)diazen-1-ium-1,2-diolate) were approximately 1.5 and 7.5 μM, respectively. (**a**) Spectral changes of the NO binding to HsGCβ195, insets show detailed spectral changes in the whole process; (**b**) spectral changes of the NO binding to HsGCβ619

estimated. For HsGCβ195, $k1$, $k2$, $k3$, $k4$ (as shown in Fig. 6) are >0.2, 0.02, 1.1×10^{-3}, and 2.2×10^{-4} s^{-1}, respectively. For HsGCβ619, $k1$, $k2$, $k3$, $k4$ are >0.3, 0.01, 2.4×10^{-3}, and 7×10^{-5} s^{-1}, respectively. The rate constants were summarized in Table S1, in supporting information.

The binding of NO to the heme of sGC can activate the conversion of GTP to cGMP for several hundred folds. NO binds to the heme to form a five-coordinated species (state B in Fig. 6) via iron-histidine bond cleavage, which is consistent with that in previous studies (Makino et al. 2003; Yazawa et al. 2006). The NO binding perhaps causes the conformational transformation of L2 (Loop2, residues 124–130) indicated in the homology model of human HsGCβ195 (Fig. 2). After that, the activation information is propagated from the H-NOX domain to the cyclase domain, eventually the conversion of GTP to cGMP is activated successfully.

Acknowledgments This work is supported in part by Shanghai Pujiang Talent Project (08PJ14017), the National Science Foundation of China (20771029), Shanghai Leading Academic Discipline Project (B108) and the Program for the Platform of new medicine creation (NO. 2009ZX09301-011).

References

Antonini E, Brunori M (1971) Frontiers of biology. North-Holland, Amsterdam

Autenrieth F, Tajkhorshid E, Baudry J, Luthey-Schulten Z (2004) Classical force field parameters for the heme prosthetic group of cytochrome *c*. J Comput Chem 25:1613–1622

Ballou DP, Zhao Y, Brandish PE, Marletta MA (2002) Revisiting the kinetics of nitric oxide (NO) binding to soluble guanylate cyclase: the simple NO-binding model is incorrect. Proc Natl Acad Sci USA 99:12097–12101

Bellamy TC, Wood J, Garthwaite J (2002) On the activation of soluble guanylyl cyclase by nitric oxide. Proc Natl Acad Sci USA 99:507–510

Berry EA, Trumpower BL (1987) Simultaneous determination of hemes a, b, and c from pyridine hemochrome spectra. Anal Biochem 161:1–15

Burstyn JN, Yu AE, Dierks EA, Hawkins BK, Dawson JH (1995) Studies of the heme coordination and ligand binding properties of soluble guanylyl cyclase (sGC): characterization of Fe(II)sGC and Fe(II)sGC(CO) by electronic absorption and magnetic circular dichroism spectroscopies and failure of CO to activate the enzyme. Biochemistry 34:5896–5903

Capece L, Estrin DA, Marti MA (2008) Dynamical characterization of the heme NO oxygen binding (HNOX) domain. Insight into soluble guanylate cyclase allosteric transition. Biochemistry 47:9416–9427

Cary SPL, Winger JA, Marletta MA (2005) Tonic and acute nitric oxide signaling through soluble guanylate cyclase is mediated by nonheme nitric oxide, ATP, and GTP. Proc Natl Acad Sci USA 102:13064–13069

Chen KJ, Pittman RN, Popel AS (2008) Nitric oxide in the vasculature: where does it come from and where does it go? A quantitative perspective. Antioxid Redox Signaling 10:1185–1198

Deinum G, Stone JR, Babcock GT, Marletta MA (1996) Binding of nitric oxide and carbon monoxide to soluble guanylate cyclase as observed with resonance Raman spectroscopy. Biochemistry 35:1540–1547

Denninger JW, Marletta MA (1999) Guanylate cyclase and the NO/cGMP signaling pathway. Biochim Biophys Acta 1411:334–350

Evgenov OV, Pacher P, Schmidt PM, Hasko G, Schmidt HH, Stasch JP (2006) NO-independent stimulators and activators of soluble guanylate cyclase: discovery and therapeutic potential. Nat Rev Drug Discov 5:755–768

Fan B, Gupta G, Danziger RS, Friedman JM, Rousseau DL (1998) Resonance Raman characterization of soluble guanylate cyclase expressed from baculovirus. Biochemistry 37:1178–1184

Gerzer R, Bohme E, Hofmann F, Schultz G (1981) Soluble guanylate cyclase purified from bovine lung contains heme and copper. FEBS Lett 132:71–74

Hu X, Murata LB, Weichsel A, Brailey JL, Roberts SA, Nighorn A et al (2008) Allostery in recombinant soluble guanylyl cyclase from Manduca sexta. J Biol Chem 283:20968–20977

Ignarro LJ, Degnan JN, Baricos WH, Kadowitz PJ, Wolin MS (1982) Activation of purified guanylate cyclase by nitric oxide requires heme-comparison of heme-deficient, heme-reconstituted and heme-containing forms of soluble enzyme from bovine lung. Biochim Biophys Acta 718:49–59

Ignarro LJ, Adams JB, Horwitz PM, Wood KS (1986) Activation of soluble guanylate cyclase by NO-hemoproteins involves NO-heme exchange. Comparison of heme-containing and heme-deficient enzyme forms. J Biol Chem 261:4997–5002

Karow DS, Pan DH, Davis JH, Behrends S, Mathies RA, Marletta MA (2005) Characterization of functional heme domains from soluble guanylate cyclase. Biochemistry 44:16266–16274

Kharitonov VG, Sharma VS, Magde D, Koesling D (1997) Kinetics of nitric oxide dissociation from five- and six-coordinate nitrosyl hemes and heme proteins, including soluble guanylate cyclase. Biochemistry 36:6814–6818

Kosarikov DN, Lee JM, Uversky VN, Gerber NC (2001a) Role of conformational changes in the heme-dependent regulation of human soluble guanylate cyclase. J Inorg Biochem 87:267–276

Kosarikov DN, Young P, Uversky VN, Gerber NC (2001b) Human soluble guanylate cyclase: functional expression, purification and structural characterization. Arch Biochem Biophys 388:185–197

Laidig KE, Daggett V (1996) Molecular dynamics simulations of apocytochrome b562—the highly ordered limit of molten globules. Fold Des 1:335–346

Lee YC, Martin E, Murad F (2000) Human recombinant soluble guanylyl cyclase: expression, purification, and regulation. Proc Natl Acad Sci USA 97:10763–10768

Li Z, Pal B, Takenaka S, Tsuyama S, Kitagawa T (2005) Resonance Raman evidence for the presence of two heme pocket conformations with varied activities in CO-bound bovine soluble guanylate cyclase and their conversion. Biochemistry 44:939–946

Lorkovic I, Ford PC (2000) Nitric oxide addition to the ferrous nitrosyl porphyrins Fe(P)(NO) gives trans-Fe(P)(NO)(2) in low-temperature solutions. J Am Chem Soc 122:6516–6517

Ma X, Sayed N, Beuve A, van den Akker F (2007) NO and CO differentially activate soluble guanylyl cyclase via a heme pivot-bend mechanism. EMBO J 26:578–588

MacKerell ADJ, Bashford D, Bellott RL, Dunbrack RL Jr, Evanseck JD, Field MJ et al (1998) All-atom empirical potential for molecular modeling and dynamics studies of proteins. J Phys Chem B 102:3586–3616

Mackerell AD Jr, Feig M, Brooks CL (2004) Extending the treatment of backbone energetics in protein force fields: limitations of gas-phase quantum mechanics in reproducing protein conformational distributions in molecular dynamics simulations. J Comput Chem 25:1400–1415

Makino R, Matsuda H, Obayashi E, Shiro Y, Iizuka T, Hori H (1999) EPR characterization of axial bond in metal center of native and cobalt-substituted guanylate cyclase. J Biol Chem 274:7714–7723

Makino R, Obayashi E, Homma N, Shiro Y, Hori H (2003) YC-1 facilitates release of the proximal His residue in the NO and CO complexes of soluble guanylate cyclase. J Biol Chem 278:11130–11137

Mathis KJ, Emmons TL, Curran DF, Day JE, Tomasselli AG (2008) High yield purification of soluble guanylate cyclase from bovine lung. Protein Expr Purif 60:58–63

Nioche P, Berka V, Vipond J, Minton N, Tsai AL, Raman CS (2004) Femtomolar sensitivity of a NO sensor from *Clostridium botulinum*. Science 306:1550–1553

Ohlstein EH, Wood KS, Ignarro LJ (1982) Purification and properties of heme-deficient hepatic soluble guanylate cyclase: effects of heme and other factors on enzyme activation by NO, NO-heme, and protoporphyrin IX. Arch Biochem Biophys 218:187–198

Pellicena P, Karow DS, Boon EM, Marletta MA, Kuriyan J (2004) Crystal structure of an oxygen-binding heme domain related to soluble guanylate cyclases. Proc Natl Acad Sci USA 101:12854–12859

Russwurm M, Koesling D (2004) NO activation of guanylyl cyclase. EMBO J 23:4443–4450

Sarkar O, Mathur PP, Mruk DD (2008) Nitric oxide-cGMP signaling: its role in cell junction dynamics during spermatogenesis. Immunol Endocr Metab Agents Med Chem 8:28–35

Schmidt PM, Schramm M, Schroder H, Wunder F, Stasch JP (2004) Identification of residues crucially involved in the binding of the heme moiety of soluble guanylate cyclase. J Biol Chem 279:3025–3032

Stone JR, Marletta MA (1994) Soluble guanylate cyclase from bovine lung: activation with nitric oxide and carbon monoxide and spectral characterization of the ferrous and ferric states. Biochemistry 33:5636–5640

Stone JR, Marletta MA (1996) Spectral and kinetic studies on the activation of soluble guanylate cyclase by nitric oxide. Biochemistry 35:1093–1099

Stone JR, Sands RH, Dunham WR, Marletta MA (1995) Electron paramagnetic resonance spectral evidence for the formation of a pentacoordinate nitrosyl-heme complex on soluble guanylate cyclase. Biochem Biophys Res Commun 207:572–577

Tomita T, Ogura T, Tsuyama S, Imai Y, Kitagawa T (1997) Effects of GTP on bound nitric oxide of soluble guanylate cyclase probed by resonance Raman spectroscopy. Biochemistry 36:10155–10160

Vogel KM, Hu S, Spiro TG, Dierks EA, Yu AE, Burstyn JN (1999) Variable forms of soluble guanylyl cyclase: protein-ligand interactions and the issue of activation by carbon monoxide. J Biol Inorg Chem 4:804–813

Wang-Rosenke Y, Neumayer HH, Peters H (2008) NO signaling through cGMP in renal tissue fibrosis and beyond: key pathway and novel therapeutic target. Curr Med Chem 15:1396–1406

Winger JA, Marletta MA (2005) Expression and characterization of the catalytic domains of soluble guanylate cyclase: interaction with the heme domain. Biochemistry 44:4083–4090

Winger JA, Derbyshire ER, Marletta MA (2007) Dissociation of nitric oxide from soluble guanylate cyclase and heme-nitric oxide/oxygen binding domain constructs. J Biol Chem 282:897–907

Winger JA, Derbyshire ER, Lamers MH, Marletta MA, Kuriyan J (2008) The crystal structure of the catalytic domain of a eukaryotic guanylate cyclase. BMC Struct Biol 8:42

Wolin MS, Wood KS, Ignarro LJ (1982) Guanylate cyclase from bovine lung. A kinetic analysis of the regulation of the purified soluble enzyme by protoporphyrin IX, heme, and nitrosyl-heme. J Biol Chem 257:13312–13320

Yamanaka T (1992) The biochemistry of bacterial cytochromes. Springer, New York

Yazawa S, Tsuchiya H, Hori H, Makino R (2006) Functional characterization of two nucleotide-binding sites in soluble guanylate cyclase. J Biol Chem 281:21763–21770

Yu AE, Hu SZ, Spiro TG, Burstyn JN (1994) Resonance Raman-spectroscopy of soluble guanylate cyclase reveals displacement of distal of distal and proximal heme ligands by NO. J Am Chem Soc 116:4117–4118

Zabel U, Weeger M, La M, Schmidt HH (1998) Human soluble guanylate cyclase: functional expression and revised isoenzyme family. Biochem J 335(Pt 1):51–57

Zhao Y, Marletta MA (1997) Localization of the heme binding region in soluble guanylate cyclase. Biochemistry 36:15959–15964

Zhao Y, Brandish PE, Ballou DP, Marletta MA (1999) A molecular basis for nitric oxide sensing by soluble guanylate cyclase. Proc Natl Acad Sci USA 96:14753–14758